RSC Advances

REVIEW

View Article Online
View Journal | View Issue

Cite this: *RSC Adv.*, 2024, **14**, 26308

Advances in the preparation and biological applications of core@shell nanocrystals based on quantum dots and noble metal

Xi Wang,[a] Peng Wang,[c] Meng Li *[b] and Jian Li*[a]

Core/shell structured nanoparticles (NPs) are a novel category of functional materials that have garnered widespread attention due to their advantageous preparation methods, unique characteristics, and multifunctional application prospects, which have shown significant performance in materials chemistry and many other fields, such as electronics, biomedical, pharmaceutical, optics, and catalysis. Although some reviews about core/shell NPs have been published, there is still an intense requirement for an extensive review about the updated literature and new reported core/shell nanomaterials. Colloidal quantum dots (QDs) and noble metal NPs have a very small size, which results in the large surface-to-volume ratio and under-coordinated chemical bonds. As a result, the effort on the design of core–shell structure has been essential for colloidal QDs and noble metal NPs. In this review, the core–shell structures dominated by traditional QDs and $CsPbX_3$ perovskite QDs, as well as noble metal nanocrystals (NCs) were summarized. The applications of the above core–shell structure NCs in medical or biological fields such as sensing, biological imaging, medical diagnostics and therapeutics, immunological diagnosis were discussed. The main objective of this review is to provide a better basis for the synthesis, properties, and biomedical applications of QDs or noble metal core/shell NPs, which is beneficial for the further development of QDs, noble metal NPs, and other NPs.

Received 25th July 2024
Accepted 14th August 2024

DOI: 10.1039/d4ra05386a

rsc.li/rsc-advances

1. Introduction

Coating bare core nanoparticles (NPs) enhances the dispersion and stability of the core particles, while also altering or enhancing their original properties. Due to the external coating, the optical activity and photooxidation stability are significantly improved. This presents a promising opportunity to explore the potential applications of nanomaterials in various domains.[1] The nature of core–shell structured quantum dots (QDs) is not a simple summation of shells, but rather a creative modification of these discrete systems, resulting in a wide range of performance enhancements in areas such as catalysis, labelling, optoelectronic devices, pharmaceuticals and biology. Novel constructive assemblies related to core–shell structured QDs can be made from a combination of several materials, such as carbon ribbons, carbon nanotubes, and metal or metal oxide NPs, and these designs can open up a new dimension of research in multidisciplinary science. The core–shell structured QDs are a key factor in solving the challenges encountered in the development of energy storage devices and alternative power sources. Core/shell NPs have exhibited attractive performance in many applications such as biomedicine,[2,3] catalysis,[4] electronics,[5] enhancing photoluminescence (PL), creating photonic crystals,[6] and so on. Especially in the biomedical field, the majority of these particles are used for bioimaging,[7] controlled drug release, targeted drug delivery,[7–9] cell labelling,[7,10] tissue engineering applications.[11,12]

Although some reviews about core/shell NPs have been published, an extensive review with updated literature on core/shell NPs is still desired. Among the reported nanomaterials, colloidal QDs and noble metal NPs have a very small size (generally <10 nm), which results in a large surface-to-volume ratio and under-coordinated chemical bonds. Surface atoms have high chemical reactivity to oxidation or adsorption of other foreign atoms, ionic migration and trapping of charge carriers, which have obviously influence on the chemical and physical properties of the NPs. As a result, the effort on the design of the core–shell structure was essential for colloidal QDs and noble metal NPs. The most common application of core/shell NPs were optoelectronics, catalysis, optical bioimaging, biological labelling. All of these applications mainly relied on the small-sized NPs, especially noble metals and QDs. Different to the previous reviews on core–shell structures, we mainly

[a]*Central Hospital Affiliated to Shandong First Medical University, Jinan, Shandong 250013, China. E-mail: zxyyjzlj@163.com*

[b]*Institute of Resource and Environmental Innovation, School of Municipal and Environmental Engineering, Shandong Jianzhu University, Jinan 250101, China. E-mail: mengli_ujn@163.com*

[c]*Department of Public Scientific Research Platform, School of Clinical and Basic Medicine, Shandong First Medical University, Shandong Academy of Medical Sciences, Jinan, China*

summarized the core–shell structures dominated by QDs and noble metal NCs.

QDs have garnered increasing attention from researchers. Among these materials, II–VI semiconductors such as ZnO, ZnS, CdTe, and CdS have demonstrated stable chemical and optoelectronic properties. These materials can be combined with noble metals and other substances to create various core/shell structure morphologies, which can serve as both the core and the shell. The design and production of these materials have the potential to open up new avenues of research in multidisciplinary science. These properties make them highly valuable in various fields, including light-emitting diodes (LEDs), solar cells, sensors, detectors, and catalysts. The preparation processes for these materials have become more elaborate due to advancements in nanotechnology.[1,13] When two II–VI semiconductor materials are combined to form a heterostructure, their properties can be significantly enhanced compared to a single crystal. Recent years, lead halide perovskites not only showed great application potential in photovoltaic and other optoelectronic device applications, but also performed good applications in energy conversion and biomedical directions due to their attractive properties. However, the poor stability of lead halide perovskites NCs severely limits its application research.[14–19] Preparation of robust shell encapsulation to cover $CsPbX_3$ core is important for improving the stability of lead halide perovskites.

Noble metals such as gold (Au), silver (Ag), palladium (Pd), platinum (Pt), osmium (Os), iridium (Ir), ruthenium (Ru), and rhodium (Rh) possess excellent chemical stability, corrosion resistance, electrical conductivity, ductility, and catalytic properties. Single semiconductor materials have limited catalytic ability and uncontrollable selectivity of products. However, by loading noble metal NPs onto the surface of semiconductor materials, the catalytic efficiency and selectivity of products can be effectively improved. This is because the electrons and holes generated after illumination are separated on the noble metal and semiconductor, respectively. Subsequently, chemical reactions occur in different locations, effectively preventing the recombination of electrons and holes and enhancing catalytic efficiency. Additionally, the noble metal that is loaded can also modify the catalytic products. For example, when Pt-loaded TiO_2 NPs are used, the decomposition of propyne under light can occur. This process is likely to generate hydrogenated compounds like ketone because the photogenerated electrons on the TiO_2 surface move towards Pt, which is further away from the holes. On the other hand, if a single TiO_2 nanoparticle is used, methane and ethane are more readily formed.

In this review, the core–shell structures dominated by QDs and noble metal NCs were summarized. Depending on the material properties, the core–shell structures are mainly categorized into (i) quantum dot based core–shell structures (ii) noble metal based core–shell structures, (iii) metal halide perovskites core–shell structures, (iv) quantum dot-precious metal core–shell structures. The applications of above core–shell structure NCs in medical or biological fields such as sensing, biological imaging, medical diagnostics and therapeutics, immunological diagnosis were discussed.

2. Core/shell heterostructure based on traditional QDs

2.1 Properties

Over the past decade, high quality (narrower size distribution, better stability and higher light excitation efficiency) sol–gel-like semiconductor QDs have attracted a lot of attention. They have considerable potential in many applications, such as light-emitting devices, laser emitters and biomarkers. The key parameters of photoexcited QDs are mainly the following: (1) high photoexcited quantum yield (PLQY); (2) photostability in practical applications; and (3) solubility in ideal solvents. All the above three points directly affect the passivation effect of the QDs surface overhang built. And the luminous efficiency of QDs also depends on the surrounding environment and other factors.

Core/shell QDs, such as CdSe/ZnS, exhibit improved quantum yields and photostability. The shell protects the core from oxidation and other degradation processes, resulting in brighter and more stable fluorescence. Small-sized NCs possessed a large surface area to volume ratio and this leads to a large degree of unsaturation, where junctions between particles might appear on the surface of the particles. These imperfect junctions might form unobstructed channels allowing photogenerated carriers to recombine. Therefore, effective surface passivation is crucial to obtain QDs with high photoexcited quantum yield (PLQY) and good stability. It has been shown that wrapping a layer of epitaxially grown wide bandgap semiconductor shells on the surface of QDs, *e.g.*, wrapping CdTe or CdSe cores with CdS or ZnS shells, is an effective means of electronically passivating the surface of NCs. In addition, the choice of specific band offsets between the core and shell offers the possibility to configure the bandgap, as well as influence the photovoltaic effect. Successful construction of the core/shell structure depended on two keys: a small lattice mismatch so that the defect generation rate is no greater than before the shell is encapsulated; and a solid solubility low enough to minimize core–shell interdiffusion. Core/shell NCs can also serve as donor or acceptor materials in fluorescence resonance energy transfer (FRET systems), enhancing the fluorescence signal through efficient energy transfer between closely spaced NCs.[20]

2.2 Classification

In Fig. 1, according to relative positions of the conduction and valence bands of the core and shell materials in the core–shell structured QDs, the core–shell structured QDs are usually categorized into "Type I", "Type II" "quasi-Type-II" energy band structure arrangements.[21,22] In type-I, both the electron and hole are inclined to localize within the material with a narrower energy gap. As a result, the emission energy is determined by core. The energy gradient in type-II structure tends to separate the electron and the hole on different sides of the heterointerface. The emission energy is determined by the energy difference between the conduction band edge of core and the valence band edge of shell.[23]

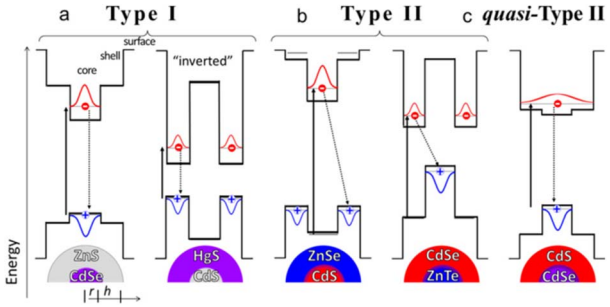

Fig. 1 (a) Type-I, (b) Type-II, and (c) quasi-Type-II band-edge alignments between the materials in core/shell QDs. Reprinted with permission from ref. 21 Copyright (2016) American Chemical Society.

In quasi-type II, the distribution of carriers is intermediate between type I and type II. One of the carriers is domain-limited in the core or shell and the other carrier is off-domain throughout the nanoparticle. In this system, it is required that the conduction or valence bands of the two have similar energy level positions, such as quasi-type II structured CdSe@CdS NCs, which are able to produce a large spectral redshift of electrons toward the shell off-domain, while having a fluorescence quantum yield close to that of type I NCs. A study by Klimov's group reported that a thin layer of ZnS shell layer grown on the surface of CdSe QDs forms a type I energy band structure in which the holes of the QDs are confined to the CdSe nucleus.[23]

In Fig. 2a and b, mono-disperse zinc blende CdSe@CdS core/shell NCs were synthesized by epitaxial growth of 1–6 monolayers of CdS shell onto zinc blende CdSe core NCs in one pot.[24] In Fig. 2(c–e), the optical properties of QDs change with the growth of the thin shell layer, indicating that the ZnS shell layer on the CdSe QDs does not change the in-band relaxation process and the complexation of the excited electrons and holes, *i.e.*, the electrons and holes of the I-type QDs are confined to the nucleus of the QDs, respectively.[25] Kambhampati investigated the dynamics of photogenerated electron complexation in CdSe@ZnS QDs and found that it was not affected by the complexation of defect states at the surface.[26] By probing the influence of the surface effect on the cooling of the in-band carriers of the QDs, it was observed that the process of the cooling of the electrons was not affected by themorphology of the surface defects, which also confirms the previously reported I-type energy band structure feature, where electrons and holes are split into two separate systems. Rosenthal *et al.* reported that the complexation efficiency of the surface trap defect states in CdSe@ZnSe QDs increases with the size of the quantum dot shell layer.[27] This is a type II or type II energy band structure.

2.3 Preparation

2.3.1 Metal–organic compound synthesis routes. There are a large number of research reports and literature about the preparation of CdSe@CdS and CdSe@ZnS core/shell structured QDs using metal–organic compound synthesis routes.[28] The general method of preparation is to synthesize the core structure first, after which it is purified and used as a seed-deposited

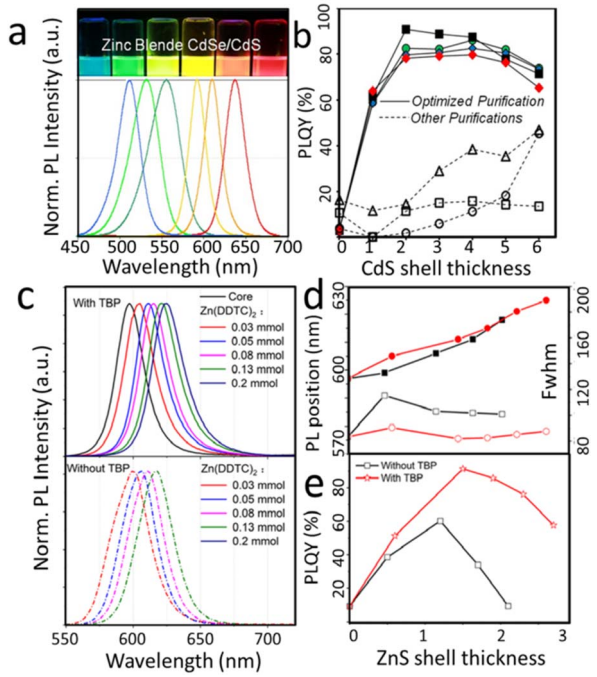

Fig. 2 (a) Luminescence pictures under UV excitation (top) and PL spectra of zinc blende CdSe@CdS core/shell NCs with different emission wavelengths. (b) PL QY *versus* shell thickness for zinc blende core and core/shell NCs synthesized under different conditions. (c) Evolution of PL spectra with different ZnS shell thicknesses in CsSe@ZnS. (d) PL properties in terms of peak position and FWHM of the emission. (e) QY value as a function of CdS shell thickness. (a and b) Reprinted with permission from ref. 24 Copyright (2012) American Chemical Society. (c and d) Reprinted with permission from ref. 25 Copyright (2022) MDPI (Basel, Switzerland).

shell material. The PLQY of CdSe@CdS and CdSe@ZnS QDs can reach at least 50% and 30–50% by shell thickness optimization. Recently, it has been reported that the PLQY of CdSe@CdS QDs can reach 97% by limiting the growth of the CdS shell and thus controlling the thickness and quality of the shell more precisely.[29] Some phosphine-free methods to prepare CdSe@ZnS NCs were reported.[30]

2.3.2 Sulfhydryl ligand-based synthetic routes. The aqueous phase method for the preparation of core/shell structured QDs is more backward compared to organic phase based methods, because the mentioned methods are generally not applicable for the synthesis of core/shell structured QDs. Water is a highly tunable solvent that readily modifies the reaction kinetics at the material surface. For example, the tendency of purified sulfhydryl-coated CdS and CdTe QDs to polymerize to form larger particles is due to the presence of a directional attachment growth mechanism for these particles when dispersed in aqueous solution.[31–33] Washing processes (precipitation, centrifugation, drying, and re-dissolution) can isolate the surface ligands to some extent, depending on the method of washing. However, the redispersion process of sulfhydryl-coated CdS and CdTe QDs also induces redistribution of the surface ligands, mainly due to the lack of equilibrium between the cations, hydroxide ions, and the coated ligands. All these

factors are detrimental to the subsequent colloidal stability of shells grown using QDs as templates. Another significant difference between the sulfhydryl ligand-based and metal–organic synthetic routes with respect to the chemistry of shell formation is that the cations and sulfhydryl-coated ligands form complex molecular-level complexes that can be mutually exclusive with the anions of the core, in particular multinuclear complexes, which caused the homogeneous nucleation of the shell material in aqueous solution. The organometallic synthesis route facilitates the deposition of the shell material rather than independent nucleation in solution, provided the precursor supply rate is sufficiently low.

By virtue of the research of Gao and colleagues,[34] a synthetic method based on the slow decomposition of sulfhydryl ligands has gradually become the dominant method for the synthesis of core/shell-structured QDs in aqueous solution. QDs with a fluorescence efficiency of 85% were synthesized using an aqueous-phase method by encapsulating a CdS shell on the surface of the CdTe core.[35] The key step in the encapsulation of the shell is the light-assisted degradation of thioglycolic acid (TGA) encapsulated on the surface of the CdTe core to slowly release S^{2-} in solution.

All QDs prepared using the aqueous-phase method have two common features: (i) no washing of the core material prior to the growth of the shell material, which is significantly different from the formation of the shell structure using the organic synthesis route; and (ii) the establishment of the core/shell structure is accomplished at the earliest stage of quantum dot formation. Indeed, the photodegradation deposition properties of TGA are significantly better than those of mercaptopropionic acid (MPA), with which it is homologous. This is further corroborated by the fact that a significant gain in luminescence efficiency over ZnSe alone can be observed by light-assisted preparation of ZnSe/ZnS after the introduction of Zn/mercaptopropionic into the solution containing ZnSe QDs.[36] In addition to the classical aqueous synthesis route, recently, Choi and his coworkers used a hydrothermal method to prepare core–shell structured QDs in aqueous solution. They used this method to prepare CdTe/CdS QDs that emit near-infrared light. In their preparation, $CdCl_2$, NaHTe and NAC were the precursor and ligand, respectively, and NAC remained as a source of S^{2-} for the growth of the shell structure at the late stage of the reaction, which was carried out at 200 °C. PLQY of the obtained CdTe/CdS QDs was enhanced to 62%, while the fluorescence excitation peak was red-shifted from 650 nm to 800 nm.[37]

2.3.3 Surface cation exchange. Cations which aggregated on anionic surfaces to form solid QDs with low solubility can form the shell structures by surface cation exchange. In contrast to the sulfhydryl ligand decomposition route, the latter is only suitable for the synthesis of core/shell structured QDs with simple common anionic structures. In addition to this, this approach may produce high-grade or subgradient core/shell heterostructures.[38,39]

At the earliest, CdS/HgS/CdS QDs were prepared by sequentially adding H_2S with Hg^{2+} to an aqueous solution containing phosphate polymer-coated CdS. Owing to the solubility product of HgS is significantly lower than CdS, the Cd^{2+} in CdS is easily displaced, but the process begins at the particle surface. The thickness of the HgS shell layer can be adjusted by repeating the substitution and redeposition process in the above steps. The thickness of the CdS shell can be adjusted without affecting the HgS shell layer by introducing additional Cd^{2+} as well as H_2S.

Surface cation exchange has also been used to prepare CdTe@HgTe core/shell structured QDs. However, once the Hg : Cd ratio reaches a certain value, the increasing concentration of Hg^{2+} in the example and the counteracting effect on the Hg : Cd ratio results in the creation of an alloy quantum dot $Cd_xHg_{1-x}Te$ with a radial concentration gradient structure, rather than the core/shell structured QDs. This phenomenon is likely to result from the fact that Hg^{2+} and Cd^{2+} have almost the same ionic radius, so that the two elements each form sphalerite structures with close lattice constants, differing by only 0.3%.[40,41]

The surface cation substitution method resulted in the formation of core/shell structures with different grades or gradients, which limits its application in the preparation of pure core/shell structured QDs, but makes it an interesting approach to control the optical properties of QDs by employing gradient or even pure alloy structures. Nevertheless, it is still technically difficult to directly map the spatial distribution of the component ions of QDs with a diameter of only a few nanometers. Many of the studies carried out so far up to this point have been based on conventional spectroscopy, but the resulting composite structures deserve to be scrutinized. In addition to steady-state spectroscopy, Rogach and colleagues have recently been working on a research approach that utilizes a combination of transient spectroscopy and theoretical studies to probe ion-exchange dynamics.[40] Lifshitz *et al.* prepared SnTe@CdTe and CdTe@SnTe Core/Shell NCs by cation exchange procedure at mild conditions combined with Kirkendall Effect.[39] Tight controlling of the reaction conditions allowed for redistribution of the elements throughout the NCs, *i.e.*, outward migration of the Sn cations while the Cd cations diffuse towards the core center. The synthesis resulted in a well-organized core/shell structure (Fig. 3).

2.3.4 Directly synthesize by cationic and anionic precursors. The direct synthesis of core–shell structured QDs in aqueous solution was carried on by introducing cationic and anionic precursors into the solution containing the core material. These (cationic and anionic precursors) were dispersed in large volumes of aqueous solution or in microdroplets controlled by surfactants, which were required to have the

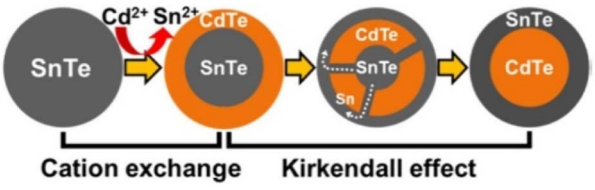

Fig. 3 Schematic illustration of the formation of SnTe-based core/shell NCs by cation exchange reaction and the Kirkendall effect. Reprinted with permission from ref. 39 Copyright (2016) American Chemical Society.

reaction conditions to enable the growth of the shell material. CdTe@ZnTe type II core–shell QDs were prepared at lower temperature by using MPA as a capping agent.[42] The thickness of ZnTe shell could be controlled by varying the precursor concentration. All changes confirmed the formation of a type II-type core–shell structure. At the chemical level, the successful preparation of core/shell-structured QDs using the reaction of an auxiliary cation/anion precursor compared to sulfhydryl ligand decomposition and surface cation exchange suggests that the direct growth of the shell structure is possible, but it depends greatly on the molecular structure of the cation/sulfhydryl complexes formed at the time of the reaction. In order to avoid uniform nucleation of the shell material during direct growth of shell structures, two approaches are often taken. One is to reduce the supply rate of the monomer, which is primarily for the formation of the nucleation/shell structure and is independent of the synthesis method, and the other is to reduce the reaction temperature.

In addition to mentioned methods, intermittent provision of small amounts of cationic/anionic precursors is also a good way to prevent uniform nucleation during shell growth. For example, Cd^{2+}-mercaptopropionic acid and HSe^{-} were sequentially added into a reaction system to grow CdSe shell structures on the surface of mercaptopropionic acid-coated CdTe QDs (emitting an orange light with a peak at 613 nm).[43–46]

There are still many challenges associated with the use of aqueous phase methods for the preparation of NCs with core/shell structures. In addition, it is difficult to individually characterize the core–shell interface in heterostructures using conventional TEM because the electron densities of group II–VI semiconductors are so different. With the development of materials testing techniques, this problem was gradually being solved. For example, core–shell CdTe/CdSe and alloy CdTeSe QDs are synthesized by aqueous solvent in 2022. TEM images showed a rod-shaped core–shell structure and an elliptical alloy structure with different crystal planes competing to grow.[47]

3. Core/shell heterostructure based on lead halide perovskites QDs

Lead halide perovskite ($CsPbX_3$) NCs have the advantages of high brightness, high defect tolerance, tunable emission wavelength, high color purity and high PLQY. Lead halide perovskites not only showed great application potential in photovoltaic and other optoelectronic device applications, but also performed good applications in energy conversion and biomedical directions in recent years. However, it is worth noting that the poor stability of lead halide perovskites NCs severely limits its application research.[14–19] Lead halide perovskite NCs would undergo degradation or PL quenching in the presence of solvents, high temperature, humidity, light illumination and O_2.[48] Preparation of robust shell encapsulation to cover $CsPbX_3$ core is important for improving the stability of lead halide perovskites.

Thermal injection and supersaturation recrystallization are commonly methods for the preparation of $CsPbX_3$ NCs. However, the stability of the prepared NCs remains poor even when the synthesis process is optimized. Preparation of robust shell encapsulation such as ZnS, SiO_2, TiO_2, Al_2O_3, $PbSO_4$, MOFs, and polymers provided the effective strategies for improving the stability of lead halide perovskites.[49–53] In Fig. 4a–c, Hou *et al.* prepared $CsPbBr_3$ core–shell structure of multidentate polymer micelles by using the copolymer template synthesis method.[54] The whole process was under room temperature. As showed in Fig. 4, the co-polymer polystyrene-*block*-poly-2-vinylpyridine was first dissolved in toluene, and then $PbBr_2$ and CsBr were added in methanol. Within the nanoshells of the copolymer polystyrene-block poly-2-vinylpyridine formed by polydentate coordination groups, a solid-phase reaction occurs, followed by crystallization to obtain $CsPbBr_3$ NCs. The polystyrene-block poly-2-vinylpyridine acted as a confined nanoreactor during the crystallization of perovskites by passivating the surface through the polydentate capping shells, which greatly enhances the photostability of chalcogenide in polar solvents. The NCs showed high stability in polar solvents and remained stable after 50 days with PL. In Fig. 4(d–h), $CsPbBr_3$@ZIF-67, $CsPbBr_3$@ZIF-8 were obtained by s directly grown of $CsPbBr_3$ in a mixture of metal ion and imidazole precursors. The prepared $CsPbBr_3$@ZIF composites improved photogenerated charge separation efficiency, CO_2 capturing ability, and moisture stability.[55]

In Fig. 5a, many studies have realized the assembly of $CsPbX_3$ into a matrix. The size of prepared composites was hundreds of nanometers. The realization of encapsulation on

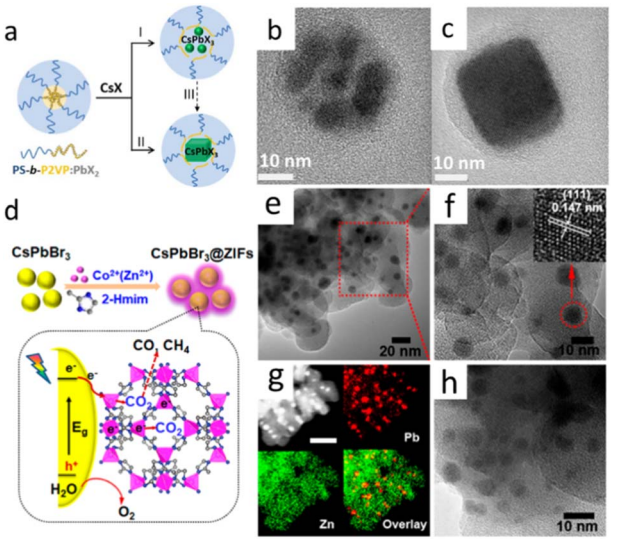

Fig. 4 (a) Synthetic strategies for perovskite NCs using amphiphilic block copolymer micelles as nanoreactors. TEM of polymer micelles containing multiple $CsPbBr_3$ NCs (b) and single $CsPbBr_3$ NC (c). (d) Schematic illustration of the fabrication and CO_2 photoreduction of $CsPbBr_3$/ZIFs. (e and f) TEM images of $CsPbBr_3$@ZIF-8. The inset of (f) is the high-resolution image of a single $CsPbBr_3$ QD marked with a red circle. (g) High-angle annular dark-field STEM image and elemental mapping of $CsPbBr_3$@ZIF-8. Scale bar: 50 nm. (h) TEM image of $CsPbBr_3$@ZIF-67. (a–c) Reprinted with permission from ref. 54 Copyright (2017) American Chemical Society. (d–h) Reprinted with permission from ref. 55 Copyright (2018) American Chemical Society.

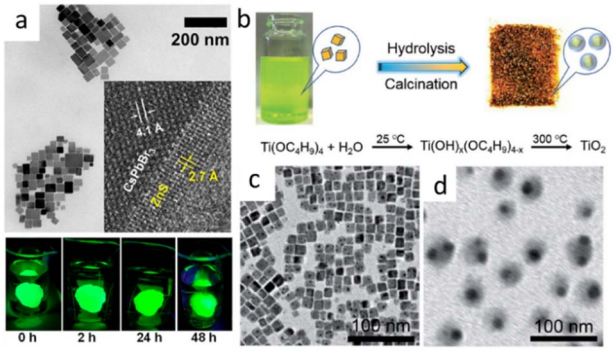

Fig. 5 (a) TEM image of $CsPbBr_3$@ZnS NCs. Inset shows HRTEM image of an NC near the core/shell interface and digital photographs of the films of $CsPbBr_3$/ZnS core/shell dipped in beakers full of water and excited with UV lamp (365 nm). (b) Schematic illustration of the fabrication process for $CsPbBr_3$@TiO_2 NCs; TEM images of $CsPbBr_3$ NCs (c) and $CsPbBr_3$@TiO_2 NCs (d). (a) Reprinted with permission from ref. 49 Copyright (2020) American Chemical Society. (b–d) Reprinted with permission from ref. 50 Copyright (2018) John Wiley & Sons.

individual $CsPbX_3$ NPs was crucial for its use in biologically fields and optoelectronic devices. Nag *et al.* prepared $CsPbBr_3$@ZnS NCs by adding extra oleylammonium bromide (OAmBr) in hot injection method. NCs maintained the high PL intensity even after being dipped in water for more than 2 days.[49] Fig. 5(b–d), Zheng *et al.* prepared $CsPbBr_3$@TiO_2 Core/Shell NCs by the encapsulation of $CsPbBr_3$ NCs with titanium precursor, followed by calcination at 300 °C.[50]

Fig. 6 showed some reported monodisperse $CsPbX_3$@SiO_2 NPs. Monodisperse $CsPbX_3$/SiO_2 and $CsPbBr_3$/Ta_2O_5 Janus NPs were successfully synthesized by combining the water-triggered transformation process and sol–gel method (Fig. 6a and b). The stability against destruction by air, water, and light irradiation was dramatically improved.[56] Li *et al.* reported a controlled

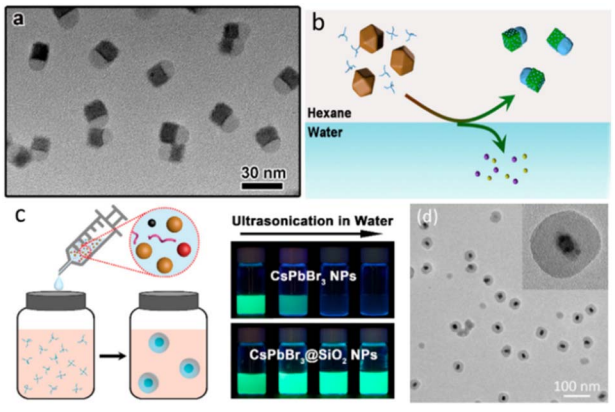

Fig. 6 (a) TEM image of $CsPbBr_3$/SiO_2 Janus NCs; (b) Schematic illustration of the formation process of $CsPbBr_3$/SiO_2 Janus NCs; (c) proposed formation process of $CsPbBr_3$@SiO_2 core–shell NPs and stability against water; (d) the TEM images of $CsPbBr_3$@SiO_2 NCs. (a and b) Reprinted with permission from ref. 56 Copyright (2017) American Chemical Society. (c) Reprinted with permission from ref. 58 Copyright (2021) Royal Society of Chemistry. (d) Reprinted with permission from ref. 57 Copyright (2021) Royal Society of Chemistry.

hydrolysis process of tetramethoxysilane to obtain the homogeneous $CsPbBr_3$@SiO_2 NCs. Firstly, Cs_4PbBr_6 NCs were silanized using partially hydrolyzed tetramethoxysilane. And then, injection of water triggered the phase transformation from Cs_4PbBr_6 to $CsPbBr_3$ and generation of condensation SiO_2 shell.[57] Another monodisperse $CsPbBr_3$@SiO_2 NCs were reported by Zhong *et al.* (Fig. 6c). One-pot synthesis method was used by precisely controlling the reaction temperature, precursor species, ligand ratio, and pH.[58] Li. *et al.* prepared a homogeneous $CsPbBr_3$@SiO_2 and Janus structure by controlling the hydrolysis process of tetramethoxysilane.[57] Table 1 is the summary of the reported $CsPbBr_3$ core–shell nanocomposites in single particle level.

4. Core/shell heterostructure based on noble metal NCs

4.1 Properties

4.1.1 Localized surface plasmon resonance (LSPR). Localized Surface Plasmon Resonance (LSPR) is a property of noble metal NCs that arises from the collective oscillation of conduction electrons when they are excited by light.[59] For core/shell NCs, where a core of one material is surrounded by a shell of another, the LSPR properties can be significantly tuned by varying the materials, sizes, and shapes of both the core and the shell. Common noble metals used include gold (Au), silver (Ag), and copper (Cu). The choice of core material affects the resonance frequency. The shell can be another metal, a semiconductor, or a dielectric material. Different materials can lead to different plasmonic behavior. The size and shape of both the core and the shell influence the LSPR properties. Smaller sizes lead to higher resonance frequencies, while larger sizes shift the resonance to lower frequencies. Shapes such as spheres, rods, cubes, and more complex geometries lead to different plasmonic modes. Coupling between the core and shell plasmons can lead to hybridized plasmon modes. This coupling can be tuned by adjusting the core/shell dimensions.

4.1.2 Surface-enhanced Raman scattering (SERS). Raman scattering is an inelastic scattering process where incident photons interact with molecular vibrations, resulting in a shift in the energy of the scattered photons. SERS is a powerful technique that enhances the Raman scattering signal of molecules adsorbed on rough metal surfaces or NPs, typically gold (Au) or silver (Ag). The enhancement is attributed to electromagnetic enhancement mechanism and chemical enhancement mechanism. Electromagnetic enhancement mechanism arises from the LSPR of metal NCs, which amplify the local electromagnetic field around the nanostructure, enhancing the Raman signal. Chemical enhancement mechanism involves charge transfer between the adsorbed molecules and the metal surface, which can also contribute to the Raman signal enhancement. When core–shell NCs are used in SERS, the Raman signal of adsorbed molecules can be enhanced. If the core or shell is the plasmonic metal (*e.g.*, Au or Ag), the NC itself can acts as a SERS substrate. For example, noble metal (like gold or silver) core/shell NCs enhance Raman signals through LSPR.

Table 1 Summary of the reported $CsPbBr_3$ core–shell NPs in single particle level

Type	Preparation method	Size (nm)
$CsPbX_3/SiO_2$ Janus	Water-triggered transformation process	Width: 11.3
$CsPbX_3/Ta_2O_5$ Janus	Water-triggered transformation process	Length: 14.7–23.9
$CsPbBr_3$@ZnS	Hot injection method with OAmBr	48.7
$CsPbBr_3$@SiO_2	Water-triggered transformation process	47 nm
$CsPbBr_3$@SiO_2	One-pot	18.2
$CsPbBr_3$@TiO_2	Calcination	Shell thick: 5 ± 3 nm

A non-metallic core (*e.g.*, silica or semiconductor) coated with a thin layer of plasmonic metal can combine the beneficial properties of both materials. The enhancement in SERS using core–shell NCs depends on core and shell material, thickness of the shell, and surface roughness and morphology. The electromagnetic field around these NPs boosts the Raman scattering of nearby molecules, allowing for detection at lower concentrations.[60]

4.1.3 Metal enhanced fluorescence (MEF). Metal-enhanced fluorescence is a phenomenon where the fluorescence properties of NCs are enhanced due to the presence of metallic NPs. Metal enhanced fluorescence was showed in Fig. 7. When fluorescent NCs are in close proximity to metal NPs, their fluorescence can be enhanced. This happens because the metal NPs can amplify the local electromagnetic field, increasing the excitation rate of the fluorophores. Additionally, the metal can modify the radiative decay rate of the fluorophores, making them emit light more efficiently. In the context of core@shell NCs, MEF can be achieved by placing these NCs near metal NPs. The enhancement depends on several factors, including the distance between the metal and the NCs, the size and shape of the metal NPs, and the spectral overlap between the plasmon resonance of the metal and the emission spectrum of the NCs. The size of NPs determines the absorbed emission and scattering ratios, the mode of discrete excitations on the active surface, and the position of the SPR peak.[62] The shape of NPs is one of the key parameters for characterizing plasma properties.[63] The distance between the fluorophore and the metal surface is also important, and it has been suggested that MEF occurs when the fluorophore is excited near the metal surface at a distance in the range of 5–90 nm.[64–66] The thickness of shell plays a crucial role in determining the SERS and SEF properties of core–shell NPs. MEF of core@shell NCs is used to improve the brightness and detection sensitivity of fluorescent labels in various applications, such as bioimaging, sensors, and photonic devices. This enhanced fluorescence technology has been widely used in environmental analysis, biotechnology (including fluorescence imaging, immunoassay and biological mechanism research), biomedical analysis (viral and bacterial detection and clinical diagnosis) and so on.

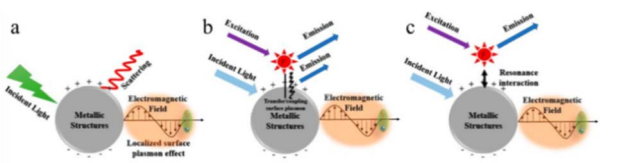

Fig. 7 Metal enhanced fluorescence mechanism: (a) the SPR effect, (b) the plasmon coupling effect due to non-radiative interactions, (c) the intrinsic radiative decay effect. (a–c) Reprinted with permission from ref. 61 Copyright (2020) Multidisciplinary Digital Publishing Institute.

Noble metal core–shell structures are materials formed by using noble metals (Au, Ag, Pt, Pb) as the core or shell, whose properties can be changed by adjusting the core–shell dimensions and chemical compositions to realize the controlled synthesis of multifunctional NPs. Using simulations and computational methodologies to examine pure Ag/Au and Ag@Au/Au@Ag core–shell NPs, it was demonstrated that even a single shell layer led to discernible changes in the electronic structure.[67] Due to the wide variety of noble metal core/shell structures and the different preparation methods as well as the properties of each aspect, several typical methods for the preparation of noble metal core/shell were introduced.

4.2 Preparation

4.2.1 Templated method. Lou[68] *et al.* used a simple template technique to synthesize hollow nanocapsules with multinuclear Au (or Pt)@SiO_2 shells, and noble metal Au or Pt NPs were located on the inner surface of the shells, and some hollow shell materials with dimer, trimer, and tetramer were obtained by the nanoparticle self-assembling process; the multinuclear Au/SiO_2 hollow particles were immersed in hydrochloric acid, nitric acid, and aqua regia, and were firstly Ostwald ripening process in the micrometer space was investigated. The advantage of this method over previous methods is that the prepared PS@Au NPs are homogeneous and stable, and the Au NPs are uniformly deposited on the surface of the PS nanotemplates, which provides good conditions for the preparation of the hollow spheres.

4.2.2 Metal seed reduction method. As mentioned before, metal seed reduction method is an effective method for the preparation of magnetic core–shell NPs, which usually uses magnetic nanoparticle solutions (*e.g.*, Co and Fe, *etc.*) as the seed solution and forms a noble metal-coated shell layer on its surface by reduction reaction. Compared with the previous methods (vacuum deposition and inverse micellar method), this method produces core–shell particles with a narrow particle size distribution, which overcomes the effect of the wide particle size distribution on the magnetic properties in the previous methods.[69]

Bao *et al.*[70] synthesized Co@Au core–shell NPs with magneto-optical properties by using the weak reduction of octadecylamine to reduce the organic gold compound on the surface of Co species in the nonpolar solvent toluene. The homogeneous and well-crystallized shell layer is more easily prepared in the presence of weak reducing agent octadecylamine and nonpolar solvent, while Au as the shell layer can provide good biocompatibility and near-infrared optical activity. Dai *et al.*[71] prepared the ternary metal Pt@Co-core Au-shell NPs by reduction of $HAuCl_4$ solution with $NaBH_4$ in Pt@Co seed solution, and heat-treated them to obtain core–shell NPs in face-centered tetragonal phase. Ban *et al.*[72] first reduced $FeCl_3$ with Na in NMPO (1-methyl-2-pyrrolidinone) solvent to obtain a black-brown solution of Fe core particles, added a certain amount of 4-phenylpyridine protector to continue the reaction for a certain period of time, and added dropwise NMPO solution containing $HAuCl_4$ to the core particle solution, and used the surface of the core particles to self Au^{3+} was reduced by the reduction of the surface of the core particles, and Au-coated Fe NPs were formed. Analysis showed that the coating of Au did not affect the magnetic properties of the core particles, and the surface plasmon resonance absorption peaks of core–shell NPs after the coating underwent an obvious red-shift phenomenon, which was shifted from 520 nm to 680 nm.

4.2.3 Sol–gel method. The sol–gel method is a common method for the preparation of noble metal/oxide (where the oxides are ZrO_2, TiO_2, Fe_2O_3, and SiO_2, *etc.*, and the noble metals are Au, Ag, *etc.*).[73–76] Typical core–shell NPs are usually synthesized by using chemical reduction method, and then it is used as a seed for the hydrolysis of metal–organic salts on the surface of the noble metal/oxide core/shell NPs. The advantage of this method is that the oxide shell layer is easy to control, and different thicknesses of the shell layer can be obtained by controlling the factors including coating time, concentration of reactants, catalyst, and other precursors. Sakai *et al.*[75] prepared $Ag@TiO_2$ core–shell NPs by sol–gel reaction of TiO_2 on the surface of Ag particles by adding $AgNO_3$ solution to CTAB solution and hydrazine hydrate to reduce Ag particles at room temperature and then added ethanol-TTIP solution.

4.2.4 Chemical reduction method. Gold coating on core NPs improved many physical properties, such as the chemical stability, the biocompatibility and bioaffinity, and the optical properties.[77,78] The optical response of Au nanoshells can be tuned in the visible to near-infrared region by varying the relative size of the core nanoparticle and the thickness of the gold shell.[79] The result showed that the gold nanoshell may prove useful for biomedical imaging applications. Chemical reduction method is a common method for the preparation of oxide@noble metal (where the oxides are SiO_2, SnO_2, TiO_2, Fe_2O_3 and Fe_4O_3, *etc.*, and the noble metals are Au, Ag, Pd, *etc.*).[80–82] This method differs from the sol–gel method in that it is a reverse encapsulation process using the oxides as the core. The preparation process usually starts with surface modification of the oxide surface using organic substances, so that the surface carries some functional groups that are easy to connect with noble metals, and then the noble metals are immobilized on the surface of the oxide through chemical bonding, and then the oxide/noble metal-type core–shell NPs are obtained by the chemical reduction method; the ions containing noble metals can also be adsorbed on the surface of the oxide through simple electrostatic interaction, and then the oxide/noble metal-type core–shell NPs can be prepared through a further the oxide/noble metal-type core–shell NPs can also be prepared by simple electrostatic adsorption of noble metal-containing ions on the surface of the oxide by further chemical reduction reaction.

Lei and colleagues prepared $SnO_2@Ag$ and $SnO_2@Au$ core–shell NCs using a seed-mediated hydrothermal method.[83,84] Hollow SnO_2 NPs were first prepared by using SiO_2 as a seed. SnO_2 was then used as a seed to prepare $SnO_2@Ag$ with $SnO_2@Au$. The test results of photodegradation rhodamine B experiments demonstrated that the photocatalytic properties of SnO_2 were significantly improved after loading Ag and Au.[85] In 2016, the $Au@SnO_2@Ag$ and $Au@SnO_2@Au$ yolk–shell NPs are synthesized *via* a silica seeds-mediated hydrothermal method. The catalytic results showed the synergistic effect of Au and Ag in the metal–semiconductor core shell structures, which was beneficial to the catalytic reduction of 4-nitrophenol into 4-aminophenol.[86] It was shown that NPs with this structure directly affect the photophysical and photocatalytic properties of metal and semiconductor nanoclusters and enhance the rate of surface charge migration. Au@Pt NPs were synthesized by reducing $HAuCl_4$ and H_2PtCl_6 with sodium citrate and ascorbic acid (AA).[87] The prepared Au@Pt core/Shell NPs were used as the probe for versatile barometer biosensor.[88] Lu *et al.* reported a novel strategy for the preparation of Au@N-CQDs@Pt NPs by reducing $HAuCl_4$ with N-CQDs at 100 °C and reducing H_2PtCl_6 with AA. The remarkable advantage of the protocol was no stabilizer or surfactant agent used.[89]

4.2.5 Laser-assisted synthesis. Laser-assisted synthesis is a new method for the preparation of magnetic core–shell NPs in recent years, which has been widely recognized by researchers, and the advantage of this method lies in the long-term oxidation resistance of the prepared particles. Zhang *et al.*[90] used laser-assisted synthesis to prepare Fe@Au NPs. Firstly, octyl ether solution containing oleic acid was heated under stirring, and a certain amount of $Fe(CO)_5$ was injected to synthesize monodispersed Fe core NPs by wet chemistry; cyclohexane solution containing Fe core NPs was added to the solution containing Au powder-water-octane, and cationic surfactant CTAB was used as a liquid-phase stabilizer, and *n*-butanol was used as a co-surfactant, and the mixture was then irradiated with a laser, which caused the reaction to produce Fe@Au core–shell NPs. The prepared core–shell particles have superparamagnetic and long-term oxidation resistance at room temperature and high saturation magnetization strength compared with other iron oxides and magnetic materials, which are expected to be applied in medical diagnosis.

Gamma (γ)-irradiation is also a method for realizing core–shell structures when polymers are encapsulated on top of noble metal NPs. The method involved the use of γ-irradiation to trigger a conventional free radical polymerization process of pure organic NPs and nanocomposites.[91] For example, PANI γ-irradiation-induced polymerization enabled the preparation of

Ag@PANI.[92] The γ-irradiation triggered the interaction of aniline (ANI) and $AgNO_3$, where Ag^+ acted as an electron acceptor and is reduced when the ANI monomer was oxidized. Initial irradiation decomposes NO_3^- ions in $AgNO_3$, triggering polymerization of the ANI monomer. Subsequently, Ag^+ oxidized the residual oligomers, dimers, or tetramers. This complex oxidation and reduction interaction produced Ag@PANI core–shell NPs.

In addition to the above methods, there are also diffusion methods, heat treatment methods and so on, which are not introduced here. Some researchers have also selected two or more of the above methods and used them in combination, and have also achieved remarkable results.

5. Core/shell heterostructure based on QDs and noble metal NCs

Noble metal/semiconductor heterostructures have attracted the attention of lots of researchers due to their wide range of applications in the field of degrading organic pollutants. The noble metal@semiconductor hybrid NPs may maintain and further improve the properties of the individual components and even generate new synergistic effects. These properties might originate from the interface between the noble metal and the self-semiconductor. Recently, colloidal NPs with a variety of materials have been prepared by a controlled synthesis process to obtain a variety of nanoscale metal/semiconductor mixture heterostructure systems, such as dumbbell, two-sided, core/shell, and yolk/shell structures. It is shown that the loading of noble metals can effectively prevent carrier recombination between the metal and the semiconductor and improve the light trapping efficiency, thus enhancing the photocatalytic performance of the materials. In addition, the semiconductor contact can improve the plasmonic properties of metal nanostructures. This phenomenon occurs through coupling of surface plasmon or modification of the local dielectric environment. Due to the intrinsic surface plasmon resonance effect, these materials exhibit size-dependent optical properties.

Metal/sulfur semiconductor core–shell structured NCs have been widely studied as a typical material system of surface plasmonic excitogen-exciton coupling interaction.[93,94] Zhang *et al.* reported the non-epitaxial preparation of metal/semiconductor heterogeneous core–shell NCs with large lattice mismatch degree and their novel applications in light-matter-spin precise modulation.[95] Compared with oxide semiconductors, II–VI semiconductors have narrower forbidden bandwidths and better absorption properties for visible light, which have unique advantages and theoretical, applied research value in photovoltaics, photocatalysis, and so on.

Zhang *et al.*[95] proposed a novel non-epitaxial growth method and combined it with the cation exchange method to successfully prepare Au@CdS core–shell structures with a single shell layer. And after that, Au@CdS core–shell NCs were further studied using this method and found that such metal@-semiconductors synthesized by the non-epitaxial growth method with a single-crystal shell layer can be used to flexibly and controllably control plasmonic resonance-exciton coupling and prolong the lifetime of excitons.[96–98] In Au@CdS NCs, the semiconductor CdS forms a shell layer in direct contact on the surface of the Au core in both dimensional directions. In this way, the disadvantage of enhanced photocatalytic performance of some particles out of the field due to surface plasma-induced electromagnetic field enhancement of the heterogeneous structure because of the directionality of the surface plasma magnetic field is avoided, resulting in high catalytic performance for each nanocrystal, and leading to an increased separation of photogenerated electrons from holes.

6. Biological application

Core–shell NPs have good advantages in biological applications, such as their lower cytotoxicity, better dispersion and biocompatibility, easier binding to bioactive molecules, better thermal and chemical stability. When the desired NPs are toxic, it may cause a lot of trouble to the host tissues and organs. Coating the core surface with a layer of harmless material makes the NPs much less toxic. The shell layer not only serves as a non-toxic layer, but also improves the performance and stability of the core material. The core–shell structure can also improve the hydrophilic and hydrophobic properties of the core material and achieve better biocompatibility. In addition, the core–shell structure allows for the binding of specific types of biomolecules. Therefore, core–shell NPs are more promising for biological applications than bare NPs. The summary of the typically biomedical application of core–shell NPs was illustrated in Fig. 8.

6.1 Sensing

The size and shape dependent QDs with color tunability confirming the significant influence in a biological system and considered as ideal probes. The former study confirmed that core–shell QDs exhibited the stronger PL and smaller full-width-half-maximum (FWHM) than bare QDs, suggesting that the core–shell QDs have the nearly uniform size distribution and good dispersion. The quantum yield (QY) of the core–shell QDs is increased by surface passivation.[99] CdSe@ZnS core–shell structured QDs can be used as probes for FRET detection of

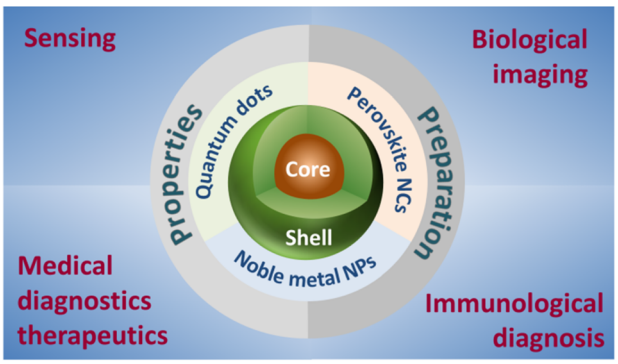

Fig. 8 Summary of the typically biomedical applications of core–shell NPs.

blood glucose when they interact with different enzymes such as glucose oxidase. The enzyme breaks down glucose through a redox reaction in which the QDs provide electrons while the enzyme acts as an electron acceptor.[100] The QDs transfer out non-radiant energy to quench the fluorescence, which corresponds to the concentration of glucose in the system. Similarly, hydrogen peroxide can be characterized by the fluorescence burst of CdSe@ZnS QDs. The emergence of such QDs makes it possible to provide a theoretical basis for an integrated nanohybrid sensor with biocatalyst and fluorescent labelling. The sensing system has an approximate fluorescence quantum yield of 20% and excellent photostability. Core–shell structured QDs have been used for optical detection of glucose in the presence of glucose oxidase.[101] The use of CdSe/ZnS core–shell structured QDs for the detection of urea when urease was used as a catalyst was reported in another study.[102] This detection was based on the enhancement of fluorescence corresponding to the rate at which urea was degraded.

Core–shell structured QDs have likewise been shown to be pH receptors, such as surface-modified CdSe@ZnS QDs.[103] pH sensing is based on the opening of the 1,3-oxazine ring after acid or base stimulation. In the former low case, a color-carrying group (4-nitrophenyl-azophenolate) is produced by the chemical stimulation, and photogenerated electrons migrate from the quantum dot to the color-carrying group and attach to its surface, leading to quenching of the quantum dot luminescence. Since ring opening of the 1,3-oxazine ring can only occur under acidic pH conditions, the color-carrying group does not absorb visible light after its formation. Since the color-carrying group does not absorb the excitation energy of the QDs, it is an electron-poor donor, which results in an increase in quantum yield. In addition, FRET-based pH receptors are reported to consist of an amphiphilic polymer core with a pH-sensitive arylturnip acid dye wrapped around the outside, and the absorption spectra of such dyes are governed by changes in pH, so that the overall absorption spectra of the sum-shell-structured QDs also vary with pH.[104]

According to the sensing strategy, noble metal NPs sensors can be categorized as colorimetric, fluorescent, electrical and electrochemical, surface plasmon resonance, and surface enhanced Raman scattering (SERS). Different types of nanobiosensors relied on different properties of noble metal NPs, such as visible color change, fluorescence quenching, surface plasmon resonance, and SERS properties. LSPR properties make core/shell NCs useful in biological and chemical sensing, as changes in the local environment can be detected through shifts in the resonance wavelength. Using Ag nanowire (NW) @ZIF-8 Core@Shell NPs, Zhang *et al.* explored the intricate interactions between the shell thickness, spatial and energetic arrangements between probe molecules and Ag NW @ZIF-8 Core@Shell NPs core–shell substrates during SERS. The results confirmed the critical role of shell thickness in influencing the sensitivity and selectivity of SERS.[105] The same result was found in Ag@SiO_2 core–shell NPs.[106] Liu *et al.* established a simple strategy for label-free SERS bioanalysis to analyze intracellular composition profiles based on Au@carbon dot (Au@CDs) nanoprobes.[107] Utilizing SERS properties, core–shell structures can also be used for the detection of antibiotic pollutants in food. For example, Yang *et al.* designed Ag@inositol hexaphosphate@Au NPs to be used as the SERS substrate, which was realized to achieve the detection of trace penicillin G in milk. The large surface plasmon resonance of the hot spot field generated in the core–shell molecular gap extends to the surface of the NPs, leading to a synergistic enhancement of the Raman scattering effect.[108] Recently, it was reported that $CH_3NH_3PbBr_3$@Al_2O_3 core–shell NPs showed excellent uniformity and reproducibility in SERS measurements, which provided the foundation for the practical application of perovskite-based SERS probes in the biological fields.[109]

By capping a SiO_2 shell layer of different thicknesses on the surface of Ag noble metal NPs, not only can fluorescent NPs with good dispersion and optical stability be obtained, but also their metal-enhanced fluorescence and the sensing properties of individual NPs can be fully utilized. MEF is a well-established technology, which can greatly enhance the fluorescence effect through the interaction between fluorescent substances and metals, improve the optical stability, reduce the scintillation of single-molecule fluorescence spectra, and decrease the fluorescence lifetime with the increase of the radiative decay rate of the system, and at the same time increase the transmission distance due to the transfer of fluorescence resonance energy. Different fluorescence probing experiments are carried out using this core–shell: organic fluorescence and lanthanide hybridization probing (non-covalent linkage), organic fluorescence covalent linkage probing. The results show that the fluorescent NPs with the core–shell structure have a 20-fold enhancement of their fluorescence signal and a 200-fold increase in the detectability of the particles compared to fluorescent NPs.[110] Tang *et al.* fabricated Ag@SiO_2@SiO_2-RuBpy core–shell NPs for the detection of prostate-specific antigen (PSA) in both buffer and serum. PL enhancement of core–shell NPs was up to 3-fold when the separation distance between the surface of silver core and the center of the third RuBpy doped silica shell is about 10 nm (Fig. 9).[111] In 2023, Maquieira *et al.* prepared $CsPbX_3$@SiO_2 core–shell NPs and successfully demonstrated their specific recognition of a humanized

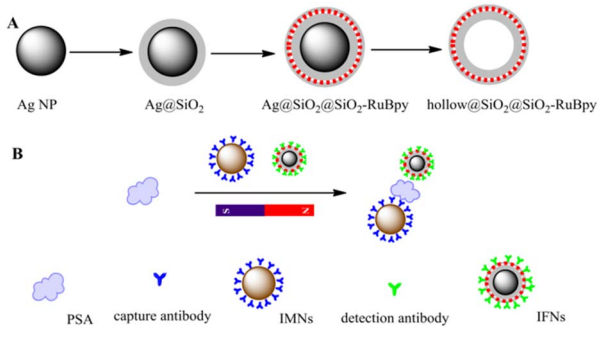

Fig. 9 (A) Schematic illustration for synthesis of Ag@SiO_2@SiO_2-RuBpy and hollow@SiO_2@SiO_2-RuBpy. (B) Schematic illustration for the construction of the detection of PSA with the immunomagnetic nanospheres and immunofluorescent NPs. Reprinted with permission from ref. 111 Copyright (2017) Elsevier.

antibody (omalizumab) used in treating patients with severe allergic asthma.[112] Sun *et al.* designed a sandwich-type electrochemical sensor for highly sensitive detection of alpha-fetoprotein (AFP) based on aptamer (Apt)-AFP-Ab interaction mode with Ag@Au core–shell NPs as a signal amplifier.[113] The novel sandwich-type electrochemical sensor peroformed the high sensitivity, outstanding selectivity, and promising application prospect in bioanalysis.

Overall, the tailored optical properties of core/shell NCs significantly enhance their utility in analytical and biomedical applications, providing more sensitive and reliable detection methods.

6.2 Biological imaging

Core@shell NCs are widely used in bioimaging due to their superior fluorescence properties. QDs with a CdSe core and a ZnS shell, for example, exhibit high brightness and photostability, making them ideal for long-term imaging of biological specimens.

Their tunable fluorescence properties make them ideal for biolabeling applications, allowing for specific tagging of cells or proteins and subsequent imaging for research and diagnostic purposes. Large number of researches applied QDs in biological imaging.[72,114,115] Compared to the traditional dyes, QDs core–shell NCs possessed some special optical properties in biological imaging, such as higher extinction coefficients; higher PLQYs; less photobleaching; absorbance and emissions can be changed with size; broad excitation band narrow emission peaks; multiple QDs can be used in the same assay with minimal interference with each other. Table 2 lists the studies of QDs for *in vivo* and *in vitro* imaging and diagnostic applications according to UV-NIR tunable fluorescence, FRET, charge transfer, and surface-enhanced Raman spectroscopy (SERS).[116,117]

Recent years, $CsPbBr_3$ have emerged as new class of candidate for many biomedical applications, such as ultrahigh-resolution bioimaging, biosensing, and flow cytometry, owing to their excellent PL properties.[118–120] $CsPbBr_3$ NCs and hollow graphitic carbon nitride nanospheres nanocomposite was prepared as DNA probe for the estimation of CD_{44} expression on the MCF-7 cell surface (Fig. 10a).[118] Park *et al.* prepared $CsPbBr_3@SiO_2$ core–shell NPs for cell imaging and drug delivery (Fig. 10b). The results demonstrated $CsPbBr_3@SiO_2$ NPs were nontoxic, making them available for *in vitro* cell imaging. Using doxorubicin, it was confirmed that $CsPbBr_3@SiO_2$ NPs can be used for drug loading and delivery.[121] In 2024, $CsPbBr_3@SiO_2$ performed the high biocompatibility and

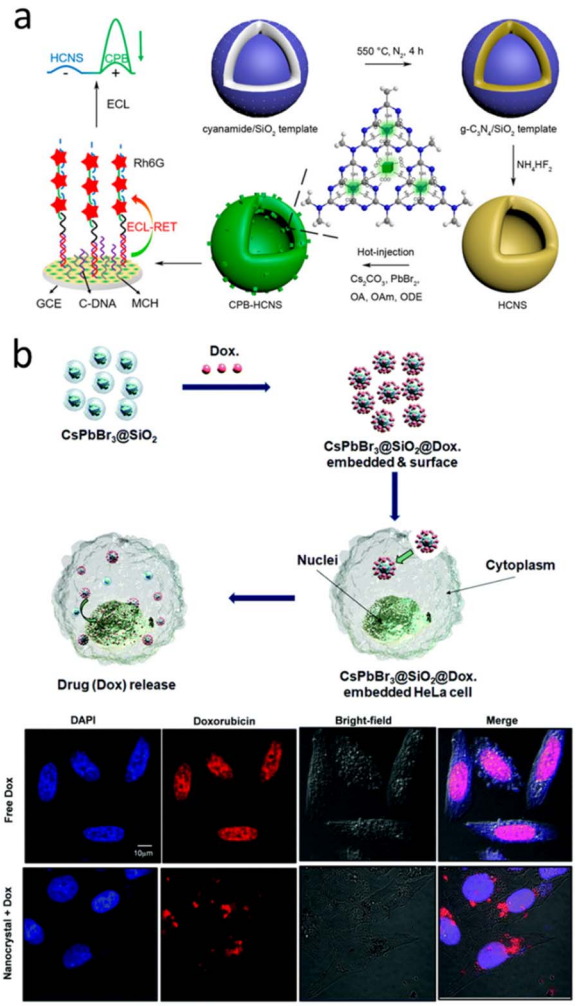

Fig. 10 (a) Schematic Illustration of the *in situ* assembly of $CsPbBr_3$ NCs into hollow graphitic carbon nitride nanospheres as the DNA probe for the targeting of CD_{44} receptors on the MCF-7 cell surface and the double signal amplification. (b) Schematic of the proposed mechanism of drug loading and release in the $CsPbBr_3@SiO_2$@Dox-embedded HeLa cells, as well as the confocal fluorescence image of HeLa cells after incubation with Dox-loaded $CsPbBr_3@SiO_2$ core–shell NCs. (a) Reprinted with permission from ref. 118 Copyright (2020) American Chemical Society. (b) Reprinted with permission from ref. 121 Copyright (2020) Royal Society of Chemistry.

Table 2 Selected *in vitro* and *in vivo* bioimaging studies using QDs

Type	Application	Techniques	Emission
$CdSe@CdS@SiO_2$	Mouse fibroblast cell imaging	*In vitro* fluorescence	550 nm & 630 nm
CdSe@ZnS	Biological detection/sensing	*In vitro* fluorescence	
$CdSe@ZnS@SiO_2$	Phagokinetic track imaging	*In vitro* fluorescence	554 nm & 626 nm
CdSe@ZnS	Tumor vasculature and lung endothelium imaging	*In vitro* and *in vivo* fluorescence	<10 nm
CdTe@CdSe	Cancer cell lymph nodes imaging	*In vivo* fluorescence	Near infrared
CdSe@ZnS	Maltose binding protein	*In vitro* FRET	560 nm
$CsPbBr_3@SiO_2$	Bioimaging	*In vitro*	518 nm

showed the great application potential in the field of bioimaging.[122]

Used in drug delivery and imaging, Au@silica core–shell NPs leverage the biocompatibility of silica and the unique optical properties of gold. Noble metal core–shell NPs performed enhanced properties and functionality because of their special use in medical imaging, such as X-ray and optical imaging, and fluorescence.[123]

6.3 Medical diagnostics and therapeutics

Hussain *et al.* reported a one-pot method for the preparation of InP@ZnS QDs with controllable morphology, size and fast reaction at low temperature. The prepared QDs can be tuned from the blue region to the near infrared and can be used as cellular fluorescent probes after surface modification.[124] By virtue of the plasmonic properties, the fluorescence peak position of Fe_3O_4@Au and Fe_3O_4@Au@Ag core–shell structured QDs can be arbitrarily red-shifted to 560 nm or blue-shifted to 501 nm by varying the thickness of the shell layer. This unique magnetic and optical properties has a great potential for applications in the field of biomedical applications, such as magnetic resonance imaging, photothermal therapy, controlled drug delivery, protein separation, biosensors, DNA detection, and immunosensors.[82,125] By functionalizing the shell with specific ligands, these NCs can target particular biomolecules or cells, enhancing the sensitivity of SERS for biomedical diagnostics. In addition, core/shell structures can be designed to provide Raman signals along with other imaging modalities, offering comprehensive diagnostic capabilities. Tian *et al.* demonstrated Au@MIL-88(Fe) NPs exhibited high performance in various diagnosis imaging methods, especially potentially allowing decreased levels of exposure of stroke patients to CT imaging radiation (Fig. 11).[126] In 2019, multi-functional Fe_3O_4@Au NPs were synthesized for cancer diagnosis and therapy. The Fe_3O_4@Au-doxorubicin-mPEG/PEG-folic acid NPs performed the increased cellular uptake through a folate-receptor-mediated endocytosis, resulting in the improved cytotoxic effect on the cancer cells. Under the laser irradiation, the cytotoxicity of Fe_3O_4@Au-DOX-mPEG/PEG-FA NPs was enhanced owing to the photothermal effect of Au shell.[127] The noble metal core shell NPs have been used in the surgical treatment of tumors as well as in the imaging of lymph nodes in large mammals, sometimes with the attachment of a polydentate phosphate coating in order to improve their solubility, stability, and dispersion in serum.[128] The biocompatibility and functionalization potential of core@shell NCs allow for the targeted delivery of therapeutic agents.

Thermal plasma NPs provided a novel and important avenue for photothermal therapy in medicine. Most of the reported core–shell NPs are spherical. In recent years, exploration of non-spherical (spherical, rod, cubic, *etc.*) core–shell NPs has confirmed their unique properties.[129–133] For example, the anisotropic shape of rod-shaped core–shell NPs can affect interactions with light.[134] Star-shaped core–shell NPs showed the larger specific surface area and distinctive SPR, which makes them valuable in catalysis and sensing applications.[135,136]

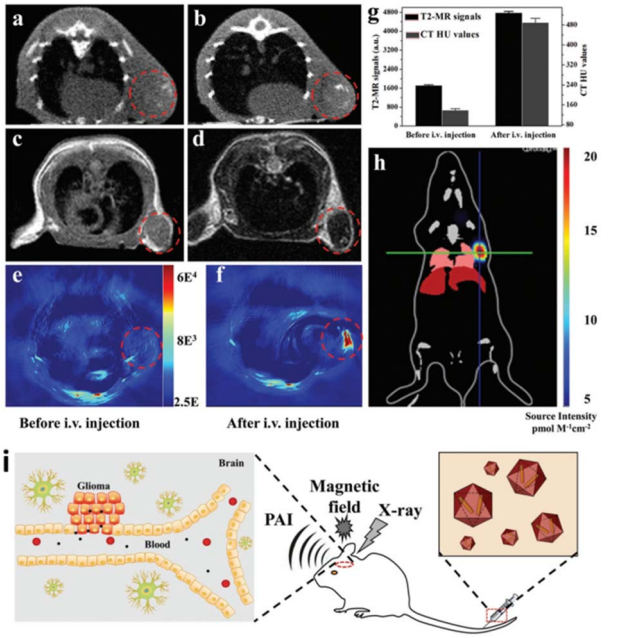

Fig. 11 *In vivo* triple-modality imaging of U87MG-subcutaneous tumor-bearing mice. (a and b) CT images of mice before and 12 h after i.v. injection with Au@MIL-88(Fe); (c and d) T_2-weighted MR images of mice before and after i.v. injection with Au@MIL-88(Fe); (e and f) *in vivo* PA imaging of tumors in mice before and 12 h after i.v. injection with Au@MIL-88(Fe); (g) quantified MRI and CT signals of tumors from mice before and 12 h after i.v. injection with Au@MIL-88(Fe); (h) bioluminescent imaging of tumor. (i) Schematic illustration of the Application to multimodality imaging-based tumor diagnosis. (a–i) Reprinted with permission from ref. 126 Copyright (2017) John Wiley & Sons.

The special geometry in the structure of gold nanorods gives it a great advantage in biosensing, imaging and diagnostic applications. Wang *et al.*[76] used a modified Stöber method to uniformly coat Au nanorods with a layer of SiO_2, which was self-assembled on PVP-modified silicon wafers to form a homogeneous Au rod@SiO_2 membrane, and the amino groups on the membrane could be covalently linked to sheep anti-human immunoglobulin forming a covalent linkage, providing a good reaction model for color detection of IgG. More impressively, the protein recognition process on the Au rod@SiO_2 membranes can be monitored either by visual observation or by changes in light absorption. Wu *et al.* designed a TiN@Au core–shell nanorod. The photothermal properties of the nanorod in the near-infrared (NIR) band were investigated using COMSOL Multiphysics software and finite element method. The results show that the TiN@Au and Au@TiN core–shell structures exhibit better photothermal properties than pure TiN nanorods of the same volume in the NIR band.[137] AuNC@CPs (Au nanocages@polymer) were prepared by dialysis of gold nanocages and coordination polymers. Due to the excellent photothermal, photoacoustic and magnetic properties of AuNC@CPs in solution, AuNC@CPs are used for near-infrared (NIR) -driven photothermal therapy (PTT) *in vivo* under the guidance of photoacoustic (PA) and magnetic resonance (MR) imaging.[138] Due to its excellent performance, noble metal core–shell NPs

will become a promising nanoprobe in the field of therapeutics. [^{198}Au]Au@SiO_2 core–shell NPs were synthesized for hyperthermia. The resulting core–shell NPs exhibited near-infrared (NIR) absorption at 750 nm and radiochemical purity of 99.91%.[139]

6.4 Immunological diagnosis

Core@shell NCs have been increasingly utilized in immunological diagnosis due to their unique properties, such as high surface area, tunable physical and chemical characteristics, and enhanced signal sensitivity. Core@shell NCs can significantly enhance the sensitivity of immunoassays. Recent studies highlight several applications of core@shell NCs in this field. For instance, a novel electrochemical immunosensor for early breast cancer detection was developed using 3D urchin-like core–shell Au@PdCu NCs. This sensor achieved high sensitivity in detecting carbohydrate antigen 15–3 (CA15–3), a key biomarker for breast cancer.[140,141] Another study focused on the synthesis of tetrahexahedral Au–Pd core–shell NCs integrated with reduced graphene oxide (rGO). This composite was used to fabricate a highly sensitive sensor for detecting epinephrine, an important diagnostic marker in various medical conditions.[142] Au NPs coated with a silica shell can amplify the signal in enzyme-linked immunosorbent assay (ELISA) tests, allowing for the detection of lower levels of antigens or antibodies. Bifunctional core@shell Au@Pt/Au NPs are presented as novel tags in Immunosensing for the determination of an Alzheimer's disease biomarker in human plasma sample. The synergy between Au and Pt metals improved the sensitivity of the detection.[143,144] Additionally, advancements in the synthesis of core@shell NCs have led to enhanced immunological responses. For example, chiral Au@Pd NCs with intrinsic chiral surfaces have been shown to produce enantiomer-dependent immunological responses, which can be crucial for the selective targeting of specific biomolecules in immunological assays.[140] The label-free Immunosensor of gold platinum@graphene QDs (AuPt@GQDs) core–shell NPs were prepared for ultrasensitive and rapid recognition of trace levels of escherichia coli from contaminated food.[145] Core@shell NCs based on QDs are particularly promising for immunological diagnosis. The bright fluorescence of QDs can improve the sensitivity of immunoassays, enabling the detection of low-abundance biomarkers. QDs can be conjugated with antibodies or antigens to serve as fluorescent probes for detecting specific biomolecules.[146] QDs used as fluorescent labels in immunoassays provide high sensitivity and multiplexing capability due to their tunable emission wavelengths. This allows for the simultaneous detection of multiple targets in a single assay.[147] There are three types of immunoassays using QDs, which is ELISA, lateral flow assays, and flow cytometry. QDs can replace traditional enzyme-linked detection systems to provide a more stable and sensitive readout. QDs can be incorporated into lateral flow test strips for point-of-care diagnostics, offering rapid and quantitative results. In this year, Gu *et al.* obtained graphene oxide (GO)-based magnetic fluorescent nanofilm (GF@DQD-APBA) with enhanced magnetic/fluorescence properties and universal capture ability for multiple viruses through the electrostatic adsorption of one layer of density-controlled Fe_3O_4 NPs and thousands of small CdSe/ZnS-MPA QDs on a monolayer GO sheet followed by chemical coupling with APBA on the QD surface (Fig. 12).[148] QDs conjugated to antibodies can be used in flow cytometry to analyze cell populations with high sensitivity and specificity. Besides, magnetic core@shell NCs can be used to separate specific cells or biomolecules from complex mixtures. This is particularly useful in immunomagnetic separation techniques, where magnetic NPs conjugated with antibodies can isolate specific cell types from blood samples.

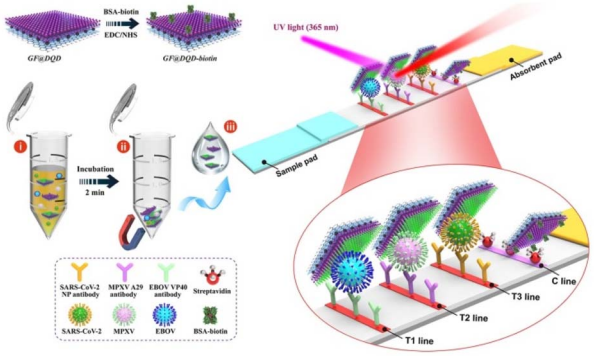

Fig. 12 Schematic of the preparation of GF@DQD biotin tag and proposed LFIA biosensor for multiplex and ultrasensitive monitoring of EBOV, MPXV, and SARS-CoV-2 antigens. Reprinted with permission from ref. 148 Copyright (2024) American Chemical Society.

These innovations demonstrate the potential of core@shell NCs to significantly improve the sensitivity and specificity of immunological diagnostics, paving the way for early and accurate detection of various diseases.

7. Conclusions and outlook

7.1 Conclusions

In this review, the core–shell structures dominated by QDs and noble metal NCs were summarized. The core–shell NCs discussed in this review have either both the core and shell made of a quantum dot or noble metal nanomaterials, or one of the core or shell structures is a quantum dot or noble metal NCs. Thus, depending on the material properties used, the core–shell structures are mainly categorized into (i) quantum dot based core–shell structures (ii) noble metal based core–shell structures, (iii) metal halide perovskites core–shell structures, (iv) quantum dot-precious metal core–shell structures. The above core–shell structure NCs performed good applications in medical or biological fields.

7.2 Perspective and challenge

It has been found that noble metal NPs and QDs have many excellent properties, and combining the unique properties with other functional materials can help to develop new materials with multi functionality and open up new applications, which has become a new hot spot in the field of nanomaterials research. At present, preliminary progress has been made on

the preparation of various noble metal or QDs core–shell NPs with different compositions and properties, but how to realize the controllable synthesis of the core particle size, shell thickness, geometric uniformity, characterization, and give full play to their multifunctionality are still the hotspots and difficulties in the current scientific research work, which still need the unremitting efforts of the majority of researchers. Core/shell heterogeneous provides a broad idea for the preparation of multi-component composites and unlimited possibilities for the development of materials science.

Among many research directions, biosynthesis in particular offers the attraction of a green bio-factory for synthesizing QDs in a mild physiological environment, thus demonstrating the biocompatibility and bio-functionality of QDs without any additional steps. An in-depth study of metal sulfide QDs has shown that the formation process still leaves much to be further explored. These would open up the possibility of preparing biocompatible QDs with tunable optical properties, especially in combination with the biological functions of natural or modified microorganisms, as a way to synthesize quantum dot probes with specific targeting functions. Currently, the latter is still in its infancy, but offers a huge scope for future research to exploit the potential of such bio-factories in advance. We hope that our efforts on this review would be able to contribute to a better understanding and further development on the synthesis, properties, and biological applications of core shell NPs.

Data availability

No primary research results, software or code have been included and no new data were generated or analysed as part of this review.

Author contributions

Xi Wang conceived the review and written the original manuscript. Peng Wang collected the literature and modified the original manuscript. Meng Li reviewed the review and provided the funding acquisition. Jian Li corrected and edited the manuscript. All authors were involved in writing and revising the manuscript.

Conflicts of interest

There are no conflicts to declare.

Acknowledgements

This work was supported by the projects from the Doctoral research fund project in Shandong Jianzhu University (X22033Z); the National Natural Science Foundation of China (No. 52270200); the Youth Innovation Technology Project of Higher School in Shandong Province (2023KJ125); The Introduction and Cultivation Plan for Young Innovative Talents of Colleges and Universities by the Education Department of Shandong Province.

References

1 A. Vaneski, J. Schneider, A. S. Susha, A. L. Rogach and J. Photoch, *Photobio. C*, 2014, **19**, 52–61.
2 S. Balakrishnan, M. J. Bonder and G. C. Hadjipanayis, *J. Magn. Magn. Mater.*, 2009, **321**, 117–122.
3 V. Salgueiriño-Maceira and M. A. Correa-Duarte, *Adv. Mater.*, 2007, **19**, 4131–4144.
4 I. V. Chepkasov, A. D. Radina and A. G. Kvashnin, *Nanoscale*, 2024, **16**, 5870–5892.
5 S. D. Adhikari, A. F. G. Reyes, S. Paul, J. Torres, B. Escuder, I. Mora-Seró and S. Masi, *Chem. Sci.*, 2023, **14**, 8984–8999.
6 P. Scodeller, V. Flexer, R. Szamocki, E. J. Calvo, N. Tognalli, H. Troiani and A. Fainstein, *J. Am. Chem. Soc.*, 2008, **130**, 12690–12697.
7 S. Laurent, D. Forge, M. Port, A. Roch, C. Robic, L. Vander Elst and R. N. Muller, *Chem. Rev.*, 2008, **108**, 2064–2110.
8 E. Yan, Y. Ding, C. Chen, R. Li, Y. Hu and X. Jiang, *Chem. Commun.*, 2009, 2718–2720.
9 A. K. Gupta and M. Gupta, *Biomaterials*, 2005, **26**, 3995–4021.
10 X. Michalet, F. F. Pinaud, L. A. Bentolila, J. M. Tsay, S. Doose, J. J. Li, G. Sundaresan, A. Wu, S. Gambhir and S. Weiss, *Science*, 2005, **307**, 538–544.
11 M. De, P. S. Ghosh and V. M. Rotello, *Adv. Mater.*, 2008, **20**, 4225–4241.
12 R. Ghosh Chaudhuri and S. Paria, *Chem. Rev.*, 2012, **112**, 2373–2433.
13 M. Kouhnavard, S. Ikeda, N. A. Ludin, N. B. A. Khairudin, B. V. Ghaffari, M. A. Mat-Teridi, M. A. Ibrahim, S. Sepeai and K. Sopian, *Renewable Sustainable Energy Rev.*, 2014, **37**, 397–407.
14 N. J. Jeon, H. Na, E. H. Jung, T.-Y. Yang, Y. G. Lee, G. Kim, H.-W. Shin, S. Il Seok, J. Lee and J. Seo, *Nat. Energy*, 2018, **3**, 682–689.
15 S. A. Veldhuis, P. P. Boix, N. Yantara, M. Li, T. C. Sum, N. Mathews and S. G. Mhaisalkar, *Adv. Mater.*, 2016, **28**, 6804–6834.
16 H. Wang and D. H. Kim, *Chem. Soc. Rev.*, 2017, **46**, 5204–5236.
17 Y. C. Kim, K. H. Kim, D.-Y. Son, D.-N. Jeong, J.-Y. Seo, Y. S. Choi, I. T. Han, S. Y. Lee and N.-G. Park, *Nature*, 2017, **550**, 87–91.
18 Q. Chen, J. Wu, X. Ou, B. Huang, J. Almutlaq, A. A. Zhumekenov, X. Guan, S. Han, L. Liang and Z. Yi, *Nature*, 2018, **561**, 88–93.
19 J. H. Heo, D. H. Shin, J. K. Park, D. H. Kim, S. J. Lee and S. H. Im, *Adv. Mater.*, 2018, **30**, 1801743.
20 Z. Li, F. Chen, L. Wang, H. Shen, L. Guo, Y. Kuang, H. Wang, N. Li and L. S. Li, *Chem. Mater.*, 2018, **30**, 3668–3676.
21 J. M. Pietryga, Y.-S. Park, J. Lim, A. F. Fidler, W. K. Bae, S. Brovelli and V. Klimov, *Chem. Rev.*, 2016, **116**, 10513–10622.
22 W. M. Girma, M. Z. Fahmi, A. Permadi, M. A. Abate and J.-Y. Chang, *J. Mater. Chem. B*, 2017, **5**, 6193–6216.

23 S. A. Ivanov, A. Piryatinski, J. Nanda, S. Tretiak, K. R. Zavadil, W. O. Wallace, D. Werder and V. I. Klimov, *J. Am. Chem. Soc.*, 2007, **129**, 11708–11719.
24 W. Nan, Y. Niu, H. Qin, F. Cui, Y. Yang, R. Lai, W. Lin and X. Peng, *J. Am. Chem. Soc.*, 2012, **134**, 19685–19693.
25 J. Li, H. Zheng, Z. Zheng, H. Rong, Z. Zeng and H. Zeng, *Nanomaterials*, 2022, **12**, 2969.
26 P. Kambhampati, *J. Phys. Chem. C*, 2011, **115**, 22089–22109.
27 M. D. Garrett, M. J. Bowers, J. R. McBride, R. L. Orndorff, S. J. Pennycook and S. J. Rosenthal, *J. Phys. Chem. C*, 2008, **112**, 436–442.
28 L. Jing, S. V. Kershaw, Y. Li, X. Huang, Y. Li, A. L. Rogach and M. Gao, *Chem. Rev.*, 2016, **116**, 10623–10730.
29 O. Chen, J. Zhao, V. P. Chauhan, J. Cui, C. Wong, D. K. Harris, H. Wei, H.-S. Han, D. Fukumura and R. K. Jain, *Nat. Mater.*, 2013, **12**, 445–451.
30 H. Shen, H. Wang, Z. Tang, J. Z. Niu, S. Lou, Z. Du and L. S. Li, *CrystEngComm*, 2009, **11**, 1733–1738.
31 J. Zheng, F. Huang, S. Yin, Y. Wang, Z. Lin, X. Wu and Y. Zhao, *J. Am. Chem. Soc.*, 2010, **132**, 9528–9530.
32 S. Yin, F. Huang, J. Zhang, J. Zheng and Z. T. J. o. P. C. C. Lin, *J. Phys. Chem. C*, 2011, **115**, 10357–10364.
33 X. Lv, X. Xue, Y. Huang, Z. Zhuang and Z. Lin, *Phys. Chem. Chem. Phys.*, 2014, **16**, 11747–11753.
34 H. Bao, Y. Gong, Z. Li and M. Gao, *Chem. Mater.*, 2004, **16**, 3853–3859.
35 P. Zrazhevskiy, M. Sena and X. Gao, *Chem. Soc. Rev.*, 2010, **39**, 4326–4354.
36 A. Shavel, N. Gaponik and A. Eychmüller, *J. Phys. Chem. B*, 2004, **108**, 5905–5908.
37 D. Zhao, Z. He, W. Chan and M. M. Choi, *J. Phys. Chem. C*, 2009, **113**, 1293–1300.
38 R. D. Robinson, B. Sadtler, D. O. Demchenko, C. K. Erdonmez, L.-W. Wang and A. P. Alivisatos, *Science*, 2007, **317**, 355–358.
39 Y. Jang, D. Yanover, R. K. Capek, A. Shapiro, N. Grumbach, Y. Kauffmann, A. Sashchiuk and E. Lifshitz, *J. Phys. Chem. Lett.*, 2016, **7**, 2602–2609.
40 S. Gupta, O. Zhovtiuk, A. Vaneski, Y. C. Lin, W. C. Chou, S. V. Kershaw and A. L. Rogach, *Part. Part. Syst. Charact.*, 2013, **30**, 346–354.
41 E. Groeneveld, L. Witteman, M. Lefferts, X. Ke, S. Bals, G. Van Tendeloo and C. de Mello Donega, *ACS Nano*, 2013, **7**, 7913–7930.
42 S. Rawalekar, S. Kaniyankandy, S. Verma and H. N. Ghosh, *J. Phys. Chem. C*, 2011, **115**, 12335–12342.
43 R. Zeng, T. Zhang, J. Liu, S. Hu, Q. Wan, X. Liu, Z. Peng and B. Zou, *Nanotechnology*, 2009, **20**, 095102.
44 Y. Xia and C. Zhu, *Analyst*, 2008, **133**, 928–932.
45 J. Wang and H. Han, *J. Colloid Interface Sci.*, 2010, **351**, 83–87.
46 Y. Zhang, Y. Li and X. P. Yan, *Small*, 2009, **5**, 185–189.
47 J. Wang, L. Wang, X. Su and R. Chen, *J. Alloys Compd.*, 2022, **920**, 165907.
48 J. Shamsi, A. S. Urban, M. Imran, L. De Trizio and L. Manna, *Chem. Rev.*, 2019, **119**, 3296–3348.
49 V. K. Ravi, S. Saikia, S. Yadav, V. V. Nawale and A. Nag, *ACS Energy Lett.*, 2020, **5**, 1794–1796.
50 Z. J. Li, E. Hofman, J. Li, A. H. Davis, C. H. Tung, L. Z. Wu and W. Zheng, *Adv. Funct. Mater.*, 2018, **28**, 1704288.
51 C. Jin, G. Kailun, Z. Yihua, Z. Jingrun, W. Yuanwei, S. Jianhua, T. Adrian, L. Chunzhong and W. Gang, *Chem. Commun.*, 2018, **54**, 8064–8067.
52 A. Loiudice, S. Saris, E. Oveisi, D. T. Alexander and R. Buonsanti, *Angew. Chem., Int. Ed.*, 2017, **56**, 10696–10701.
53 V. K. Ravi, R. A. Scheidt, A. Nag, M. Kuno and P. V. Kamat, *ACS Energy Lett.*, 2018, **3**, 1049–1055.
54 S. Hou, Y. Guo, Y. Tang and Q. Quan, *ACS Appl. Mater. Interfaces*, 2017, **9**, 18417–18422.
55 Z.-C. Kong, J.-F. Liao, Y.-J. Dong, Y.-F. Xu, H.-Y. Chen, D.-B. Kuang and C.-Y. Su, *ACS Energy Lett.*, 2018, **3**, 2656–2662.
56 H. Hu, L. Wu, Y. Tan, Q. Zhong, M. Chen, Y. Qiu, D. Yang, B. Sun, Q. Zhang and Y. Yin, *J. Am. Chem. Soc.*, 2018, **140**, 406–412.
57 M. Li, X. Zhang and P. Yang, *Nanoscale*, 2021, **13**, 3860–3867.
58 Q. Zhong, M. Cao, H. Hu, D. Yang, M. Chen, P. Li, L. Wu and Q. Zhang, *ACS Nano*, 2018, **12**, 8579–8587.
59 D. Ntirikwendera, S. Mukeshimana and J. C. Uwamahoro, *OALibJ*, 2024, **11**, e11603.
60 H. T. Beier, C. B. Cowan, I.-H. Chou, J. Pallikal, J. E. Henry, M. E. Benford, J. B. Jackson, T. A. Good and G. L. Coté, *Plasmonics*, 2007, **2**, 55–64.
61 M. A. Badshah, N. Y. Koh, A. W. Zia, N. Abbas, Z. Zahra and M. W. Saleem, *Nanomaterials*, 2020, **10**, 1749.
62 M. Rycenga, C. M. Cobley, J. Zeng, W. Li, C. H. Moran, Q. Zhang, D. Qin and Y. Xia, *Chem. Rev.*, 2011, **111**, 3669–3712.
63 T. Chung, S.-Y. Lee, E. Y. Song, H. Chun and B. Lee, *Sensors*, 2011, **11**, 10907–10929.
64 A. Puchkova, C. Vietz, E. Pibiri, B. Wünsch, M. a. Sanz Paz, G. P. Acuna and P. Tinnefeld, *Nano Lett.*, 2015, **15**, 8354–8359.
65 J.-W. Liaw, H.-Y. Tsai and C.-H. Huang, *Plasmonics*, 2012, **7**, 543–553.
66 K. Ray, R. Badugu and J. R. Lakowicz, *Langmuir*, 2006, **22**, 8374–8378.
67 L. H. dos Santos, F. D. Kiss, A. C. Ferraz and R. Miotto, *J. Phys. Chem. C*, 2024, **128**, 10751–10760.
68 X. W. Lou, C. Yuan, E. Rhoades, Q. Zhang and L. A. Archer, *Adv. Funct. Mater.*, 2006, **16**, 1679–1684.
69 V. Chiozzi and F. Rossi, *Nanoscale Adv.*, 2020, **2**, 5090–5105.
70 Y. Bao, H. Calderon and K. M. Krishnan, *J. Phys. Chem. C*, 2007, **111**, 1941–1944.
71 J. Dai, Y. Du and P. Yang, *Z. Anorg. Allg. Chem.*, 2006, **632**, 1108–1111.
72 Z. Ban, Y. A. Barnakov, F. Li, V. O. Golub and C. O'Connor, *J. Mater. Chem.*, 2005, **15**, 4660–4662.
73 P. Sudeep, K. Takechi and P. V. Kamat, *J. Phys. Chem. C*, 2007, **111**, 488–494.
74 A. S. Nair, V. Suryanarayanan, T. Pradeep, J. Thomas, M. Anija and R. Philip, *Mater. Sci. Eng., B*, 2005, **117**, 173–182.

75 H. Sakai, T. Kanda, H. Shibata, T. Ohkubo and M. Abet', *J. Am. Chem. Soc.*, 2006, **128**, 4944–4945.
76 C. Wang, Z. Ma, T. Wang and Z. Su, *Adv. Funct. Mater.*, 2006, **16**, 1673–1678.
77 J. L. Wang, Q. Fan, M. Suzuki, I. S. Suzuki, M. H. Engelhard, Y. Lin, N. Kim, J. Q. Wang and C. J. Zhong, *J. Phys. Chem. B*, 2005, **109**, 21593–21601.
78 R. Zanella, A. Sandoval, P. Santiago, V. A. Basiuk and J. M. Saniger, *J. Phys. Chem. B*, 2006, **110**, 8559–8565.
79 C. Loo, A. Lin, L. Hirsch, M.-H. Lee, J. Barton, N. Halas, J. West and R. Drezek, *Technol. Cancer Res. Treat.*, 2004, **3**, 33–40.
80 J.-H. Kim, H.-W. Chung and T. R. Lee, *Chem. Mater.*, 2006, **18**, 4115–4120.
81 L. Wang, J. Luo, M. M. Maye, Q. Fan and C. J. Zhong, *J. Mater. Chem.*, 2005, **15**, 1821–1832.
82 Z. Xu, Y. Hou and S. Sun, *J. Am. Chem. Soc.*, 2007, **129**, 8698–8699.
83 M. Lei, W. Wu, L. Sun, Q. Tian, C. Jiang and X. Xiao, *Colloids Surf., A*, 2015, **482**, 276–282.
84 K. Deng, H. Lu, Z. Shi, Q. Liu and L. Li, *ACS Appl. Mater. Interfaces*, 2013, **5**, 7845–7851.
85 W. Wu, L. Liao, S. Zhang, J. Zhou, X. Xiao, F. Ren, L. Sun, Z. Dai and C. Jiang, *Nanoscale*, 2013, **5**, 5628–5636.
86 M. Lei, W. Wu, S. Yang, X. Zhang, Z. Xing, F. Ren, X. Xiao and C. Jiang, *Part. Part. Syst. Charact.*, 2016, **33**, 212–220.
87 Z. Zhu, Z. Guan, S. Jia, Z. Lei, S. Lin, H. Zhang, Y. Ma, Z. Q. Tian and C. J. Yang, *Angew. Chem., Int. Ed.*, 2014, **53**, 12503–12507.
88 Q. Fu, Z. Wu, D. Du, C. Zhu, Y. Lin and Y. Tang, *ACS Sens.*, 2017, **2**, 789–795.
89 S. Sun, Y. Wang, T. Guo, X. Yuan, D. Zhang, Z. Xue, X. Zhou and X. Lu, *J. Alloys Compd.*, 2019, **793**, 635–645.
90 J. Zhang, M. Post, T. Veres, Z. J. Jakubek, J. Guan, D. Wang, F. Normandin, Y. Deslandes and B. Simard, *J. Phys. Chem. B*, 2006, **110**, 7122–7128.
91 M. M. Ghobashy, *Nanocomposites*, 2017, **3**, 42–46.
92 S. S. Gasaymeh and N. N. ALmansoori, *Results Phys.*, 2020, **16**, 102882.
93 S. Deka, A. Falqui, G. Bertoni, C. Sangregorio, G. Poneti, G. Morello, M. D. Giorgi, C. Giannini, R. Cingolani and L. Manna, *J. Am. Chem. Soc.*, 2009, **131**, 12817–12828.
94 J.-S. Lee, E. V. Shevchenko and D. V. Talapin, *J. Am. Chem. Soc.*, 2008, **130**, 9673–9675.
95 J. Zhang, Y. Tang, K. Lee and M. Ouyang, *Science*, 2010, **327**, 1634–1638.
96 J. Zhang, Y. Tang, K. Lee and M. Ouyang, *Nature*, 2010, **466**, 91–95.
97 Q. Zhao, M. Ji, H. Qian, B. Dai, L. Weng, J. Gui, J. Zhang, M. Ouyang and H. Zhu, *Adv. Mater.*, 2014, **26**, 1387–1392.
98 S. Lambright, E. Butaeva, N. Razgoniaeva, T. Hopkins, B. Smith, D. Perera, J. Corbin, E. Khon, R. Thomas and P. Moroz, *ACS Nano*, 2014, **8**, 352–361.
99 R. Ratnesh and M. S. Mehata, *Spectrochim. Acta, Part A*, 2017, **179**, 201–210.
100 M. N. Stojanovic and D. Stefanovic, *Nat. Biotechnol.*, 2003, **21**, 1069–1074.
101 R. Gill, L. Bahshi, R. Freeman and I. Willner, *Angew. Chem., Int. Ed.*, 2008, **120**, 1700–1703.
102 C.-P. Huang, Y.-K. Li and T.-M. Chen, *Biosens. Bioelectron.*, 2007, **22**, 1835–1838.
103 M. Tomasulo, I. Yildiz, S. L. Kaanumalle and F. M. Raymo, *Langmuir*, 2006, **22**, 10284–10290.
104 M. A. Shivkumar, L. S. Inamdar, M. H. K. Rabinal, B. G. Mulimani, G. M. A. Rao and S. R. Inamdar, *Open J. Phys. Chem.*, 2013, **3**, 40–48.
105 S. Lin, B. Chen, Y. Xu, Z. Li, Y. Liao, J. Wang, P. Yu and Y. Zhang, *Mater. Today Chem.*, 2024, **36**, 101923.
106 J. Ma, W. Yan, B. Liu and J. Yang, *J. Nanopart. Res.*, 2024, **26**, 126.
107 Y. Zheng, X. Xiao, Z. Li, Y. Shao, J. Chen, Z. Guo, H. Zhong and Z. Liu, *JoVE*, 2023, e65524.
108 T. Wang, H. Wang, A. Zhu, Y. Wu, X. Guo, Y. Wen and H. Yang, *Sens. Actuators, B*, 2021, **346**, 130591.
109 Z. Zhuang, J. Wang, J. Huang, R. Hong, C. Tao, Q. Wang, H. Lin, Z. Han, D. Zhang and S. Zhuang, *J. Phys. Chem. C*, 2024, **128**, 10120–10132.
110 K. Aslan, M. Wu, J. R. Lakowicz and C. D. Geddes, *J. Am. Chem. Soc.*, 2007, **129**, 1524–1525.
111 D.-D. Xu, Y.-L. Deng, C.-Y. Li, Y. Lin and H.-W. Tang, *Biosens. Bioelectron.*, 2017, **87**, 881–887.
112 C. Collantes, W. Teixeira, V. González-Pedro, M.-J. Bañuls, P. Quintero-Campos, S. Morais and Á. Maquieira, *Dalton Trans.*, 2023, **52**, 18464–18472.
113 X. Pei, J. Liu, Y. Zhang, Y. Huang, Z. Li, X. Niu, W. Zhang and W. Sun, *Microchim. Acta*, 2024, **191**, 414.
114 H. Zare, M. Marandi, S. Fardindoost, V. K. Sharma, A. Yeltik, O. Akhavan, H. V. Demir and N. Taghavinia, *Nano Res.*, 2015, **8**, 2317–2328.
115 J. Duan, Y. Feng, G. Yang, W. Xu, X. Li, Y. Liu and J. Zhao, *Ind. Eng. Chem. Res.*, 2009, **48**, 1468–1475.
116 S. Kim, Y. T. Lim, E. G. Soltesz, A. M. De Grand, J. Lee, A. Nakayama, J. A. Parker, T. Mihaljevic, R. G. Laurence and D. M. Dor, *Nat. Biotechnol.*, 2004, **22**, 93–97.
117 D. Bera, L. Qian, T.-K. Tseng and P. H. Holloway, *Materials*, 2010, **3**, 2260–2345.
118 Y. Cao, W. Zhu, H. Wei, C. Ma, Y. Lin and J.-J. Zhu, *Anal. Chem.*, 2020, **92**, 4123–4130.
119 H. Zhang, X. Wang, Q. Liao, Z. Xu, H. Li, L. Zheng and H. Fu, *Adv. Funct. Mater.*, 2017, **27**, 1604382.
120 X. Yang, Y. Gao, Z. Ji, L.-B. Zhu, C. Yang, Y. Zhao, Y. Shu, D. Jin, Q. Xu and W.-W. Zhao, *Anal. Chem.*, 2019, **91**, 9356–9360.
121 P. Kumar, M. Patel, C. Park, H. Han, B. Jeong, H. Kang, R. Patel, W.-G. Koh and C. Park, *J. Mater. Chem. B*, 2020, **8**, 10337–10345.
122 J. Xue, D. Chen, H. Zhang, L. Guo, P. Li, D. Han, X. Guo, Q. Duan and S. Sang, *ACS Appl. Nano Mater.*, 2024, **7**, 3997–4007.
123 N. Li, P. Zhao and D. Astruc, *Angew. Chem., Int. Ed.*, 2014, **53**, 1756–1789.
124 S. Hussain, N. Won, J. Nam, J. Bang, H. Chung and S. Kim, *Chemphyschem*, 2009, **10**, 1466–1470.

125 S. V. Salihov, Y. A. Ivanenkov, S. P. Krechetov, M. S. Veselov, N. V. Sviridenkova, A. G. Savchenko, N. L. Klyachko, Y. I. Golovin, N. V. Chufarova and E. K. Beloglazkina, *J. Magn. Magn. Mater.*, 2015, **394**, 173–178.
126 W. Shang, C. Zeng, Y. Du, H. Hui, X. Liang, C. Chi, K. Wang, Z. Wang and J. Tian, *Adv. Mater.*, 2016, **29**, 1604381.
127 S. Rajkumar and M. Prabaharan, *Colloids Surf., B*, 2019, **174**, 252–259.
128 M. H. Oh, N. Lee, H. Kim, S. P. Park, Y. Piao, J. Lee, S. W. Jun, W. K. Moon, S. H. Choi and T. Hyeon, *J. Am. Chem. Soc.*, 2011, **133**, 5508–5515.
129 J. Zhao, S. Xue, R. Ji, B. Li and J. Li, *Chem. Soc. Rev.*, 2021, **50**, 12070–12097.
130 D. Avşar, H. Ertürk and M. P. Mengüç, *J. Quant. Spectrosc. Radiat. Transfer*, 2020, **241**, 106684.
131 G. B. Kassahun, *Adv. NanoBiomed Res.*, 2019, **2**, 1–13.
132 P. Bhatia, S. Verma and M. Sinha, *Phys. Lett. A*, 2019, **383**, 2542–2550.
133 W. Brullot, R. Strobbe, M. Bynens, M. Bloemen, P.-J. Demeyer, W. Vanderlinden, S. De Feyter, V. K. Valev and T. Verbiest, *Mater. Lett.*, 2014, **118**, 99–102.
134 P. R. Sajanlal, T. S. Sreeprasad, A. K. Samal and T. Pradeep, *Nano Rev.*, 2011, **2**, 5883.
135 C. L. Nehl, H. Liao and J. H. Hafner, *Nano Lett.*, 2006, **6**, 683–688.
136 A. Silvestri, L. Lay, R. Psaro, L. Polito and C. Evangelisti, *Chem.–Eur. J.*, 2017, **23**, 9732–9735.
137 Q. Luo, Y. Liu, N. Chen and X. Wu, *Int. J. Therm. Sci.*, 2024, **204**, 109242.
138 C. Yan, L. Cui, Q. Yang, X. Zhou, L. Pan, X. Zhang, H. Yang, Z. Zhou and S. Yang, *J. Mater. Chem. B*, 2017, **5**, 8761–8769.
139 A. Fikri, L. D. Pertiwi, A. M. Forentin, D. M. Sari, S. Juliyanto, A. R. Putra, V. Y. Susilo, M. B. Febrian, H. Setiawan, A. Pujiyanto, R. Ritawidya and Y. Yulizar, *J. Radioanal. Nucl. Chem.*, 2024, DOI: **10.1007/s10967-024-09549-9**.
140 F.-X. Wu, F.-H. Li, X.-L. Lv, Q.-X. Zhang, G.-B. Xu and W.-X. Niu, *Rare Met.*, 2024, **43**, 225–235.
141 D.-N. Chen, A.-J. Wang, J.-J. Feng and T. Y. Cheang, *Microchim. Acta*, 2023, **190**, 353.
142 W. Dong, Y. Ren, Z. Bai, J. Jiao, Y. Chen, B. Han and Q. Chen, *J. Colloid Interface Sci.*, 2018, **512**, 812–818.
143 A. Iglesias-Mayor, O. Amor-Gutierrez, A. Novelli, M.-T. Fernandez-Sanchez, A. Costa-García and A. de la Escosura-Muniz, *Anal. Chem.*, 2020, **92**, 7209–7217.
144 P. Pang, X. Teng, M. Chen, Y. Zhang, H. Wang, C. Yang, W. Yang and C. Barrow, *Sens. Actuators, B*, 2018, **266**, 400–407.
145 T. Das and S. Das, *ACS Biomater. Sci. Eng.*, 2024, **10**, 4018–4034.
146 F. Ren, F. Wang, A. Baghdasaryan, Y. Li, H. Liu, R. Hsu, C. Wang, J. Li, Y. Zhong and F. Salazar, *Nat. Biomed. Eng.*, 2024, **8**, 726–739.
147 X. Shao, Z. Dong, S. Zhang, Y. Qiao, H. Zhang and H. Guo, *J. Pharm. Biomed. Anal.*, 2024, **243**, 116096.
148 C. Wang, Q. Yu, S. Zheng, W. Shen, J. Li, C. Xu and B. Gu, *ACS Nano*, 2024, **18**, 16752–16765.